"N_2O_2" Metal-azaDIPY complexes: a new class of NIR-fluorophores

Amélie Godard,[a] Laura Abad Galán,[b] Jean Rouillon,[b] Shaymaa Al Shehimy,[b] Wassima Tajani,[a] Charlotte Cave,[a] Raluca Malacea-Kabbara,[a] Yoann Rousselin,[a] Pierre Le Gendre,[a] Arnaud Fihey,[c] Mohamed Bendellaa,[d] Benoit Busser,[d,e,f] Lucie Sancey,[d] Boris Le Guennic,[c] Christophe Bucher,[b] Olivier Maury,[b] Christine Goze,[a] Ewen Bodio[a]

[a] Institut de Chimie Moléculaire de l'Université de Bourgogne, Université Bourgogne Franche-Comté, CNRS UMR 6302, Dijon, France. Mail : ewen.bodio@u-bourgogne.fr
[b] Univ Lyon, Ecole Normale Supérieure de Lyon, CNRS, Laboratoire de Chimie, UMR 5182, F-69342 Lyon, France.
[c] Univ Rennes, CNRS, ISCR (Institut des Sciences Chimiques de Rennes)−UMR 6226, F-35000 Rennes, France
[d] Univ. Grenoble Alpes, Institute for Advanced Biosciences, Inserm U 1209 / CNRS 5309, 38000 Grenoble, France
[e] Department of Clinical biochemistry, Grenoble Alpes University Hospital, 38043 Grenoble, France
[f] Institut Universitaire de France (IUF), France

Abstract:

Aza-BODIPYs are an increasingly studied class of fluorophores. They can be seen as an "aza-DIPY" ligand rigidified by a metalloid, a boron atom. Based on this idea, a series of complexes of group 13 metals (aluminum and gallium) have been synthesized and characterized. Impact of the metal and of the nature of the substituents of aza-DIPY core were investigated. The photophysical and electrochemical properties were determined and an X-ray structure of an azaGaDIPY was obtained. These data reveal that azaGaDIPY and azaAlDIPY exhibit significant red-shifted fluorescence compared to their analogue aza-BODIPY. Their emission can go up to 800 nm for the maximum emission length and up to NIR-II for the emission tail. This, associated with their electrochemical stability (no metal release whether oxidized or reduced) make them a promising class of fluorophores for optical medical imaging. Moreover, X-ray structure and molecular modeling studies have shown that this red shift seems to be more due to the geometry around the boron/metal than to the nature of the metal.

Introduction

In a few years, aza-BODIPYs have gone from being simple nitrogen analogues of the famous BODIPY fluorophores to becoming essential contrast agents for optical imaging. Indeed, these compounds are fast to synthesize at the gram scale, are chemically and photochemically stable, have good fluorescence quantum yields, and are easily functionalized.[1–4] What makes the difference between aza-BODIPYs against BODIPY dyes is their excitation and emission maximum wavelengths, which are significantly red-shifted and consequently located in the so-called biological transparency window (650-900 nm). This area of the electromagnetic spectrum corresponding to the NIR-I (Near Infra-Red I) is particularly interesting when the targeted application is *ex vivo* or *in vivo* fluorescence imaging, which is the case for example of fluorescence guided surgery (FGS). Indeed, the absorption, the scattering, and the auto-fluorescence of the biological tissues are strongly reduced in this spectral range.[5,6] This makes it possible to go from tissue thicknesses of less than one millimeter to almost one centimeter. More recently, research in optical imaging has also focused on a second window of optical

transparency, called NIR-II or SWIR for Short-Wave Infrared Region, and extends between 1000 and 1700 nm. Several biological tissues (e.g. tendons), which are still auto-fluorescent in NIR-I, are no longer so in the NIR-II optical window.[7–9] Moreover, scattering phenomena are also considerably reduced at these wavelengths, hence resulting in a much better image resolution.[6,7]

The tetraphenyl-aza-BODIPYs already emitting beyond 650 nm.[2,10] Thus, they are a particularly suitable basis for the development of new NIR-I and even NIR-II fluorophores. In the last few years, several works have been carried out in order to modulate and to increase the value of the absorption and emission wavelengths of aza-BODIPYs. Several strategies have been employed by us among others such as modifying the substituents on the aromatics surrounding the aza-BODIPY core,[11] extending the π-system,[12,13] or rigidifying the structure.[14–18] In particular, we have shown that the creation of "push->pull<-push" or "push-pull" systems allowed us to obtain emission partly in the NIR-II (Figure 1).[11,19]

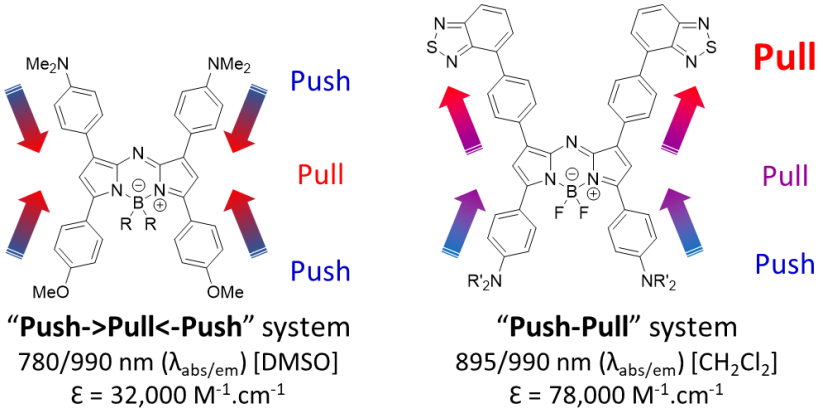

Figure 1: examples of "push-pull-push" and "push-pull" NIR-II emitting systems that we developed previously.

While most studies focus on the modification of the carbon skeleton, only a few studies concern modifications at the boron position. One of the possible explanations lies in the fact that replacing one or two fluorines by alkyl chains, alkenes or alcohols does not modify significantly the maximum absorption and emission wavelengths of the aza-BODIPYs, but lowers their fluorescence quantum yield and affects their stability.[2,20,21] In the case of substitution of boron-bearing fluorines by alkynes, the brightness of aza-BODIPYs is preserved and their stability is increased.[1,11] This is why some of us have taken advantage of these positions to water-solubilize these fluorophores and introduce different groups allowing the grafting onto vectors, the design of bimodal probes, and the conception of theranostics.[11,22–25] The only cases where the substitution of the fluorines present on the boron enabled the increase of the maximum absorption and emission wavelengths are when hydroxyls are present in *ortho* position of the aromatic rings.[26–30] In this case, the phenols chelate the boron, which stiffens the structure and significantly increases the maximum absorption and emission wavelengths.

In the present study, we are interested in the boron center itself. The presence of this atom is, indeed, justified by its capacity to rigidify the aza-DIPY core, but its electronic impact is little mentioned. We therefore wondered if its replacement by a metal could allow us to modify advantageously the photophysical properties of the fluorophore. AzaMetalDIPYs, or more simply azaMDIPYs, have already been synthesized over the last decade.[31–37] Homoleptic complexes are relatively stable, but most of azaMDIPY involving a single aza-DIPY ligand display limited stability. Moreover, their very low luminescence did not allow their use for fluorescence imaging. To increase the chance to obtain an emissive compound, we focused on aluminum and gallium because they belong to the same column as boron and should behave closer to it than other metals. This hypothesis is reinforced by the fact

that the few works that have obtained complexes with good luminescence in the case of BODIPY analogues are Al(III) and Ga(III) complexes.[38–40] To avoid the problem of stability of the complexes, we opted for an aza-DIPY substituted at the 5,5' positions by two phenate moities. In addition to stabilizing and rigidifying the species formed, this X_3L-type ligand according to Green's formalism will be particularly suitable for chelating Al(III) and Ga(III) ions.

In this study, the impact of the metal center on the photophysical and electrochemical properties will be compared with the corresponding boron derivative. Then, the impact of the substituents carried by the phenyl groups will be investigated.

Synthesis of the azaMDIPY complexes

The aza-DIPY biphenol pro-ligand was synthesized in three steps on several hundred milligrams scale by adapting procedures reported in the literature (Scheme 1).[30] This synthesis consists of a crotonization step between *ortho*-hydroxyacetophenone and benzaldehyde, followed by a 1,4-addition of nitromethane and formation of the aza-DIPY core in the presence of ammonium acetate. It is noted that the synthesis of chalcone **1** shows almost three times lower yield than in the absence of hydroxyl group in *ortho* of the ketone. This is explained by the possibility of a cyclization reaction by a nucleophilic addition of the deprotonnated phenol onto the enone.

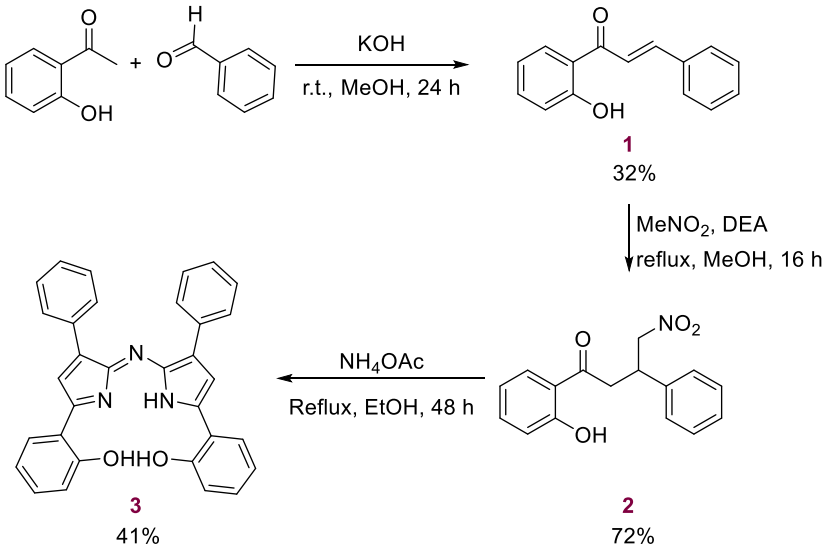

*Scheme 1: synthetic pathway of the pro-ligand aza-DIPY biphenol **3**.*

Initially, **azaBODIPY-H** was synthesized to serve as a reference compound in order to study the impact of the metal. It is obtained by reaction of aza-DIPY **3** with an excess of $BF_3.Et_2O$ in basic medium (Scheme 2). In the case of complexation with metals, two strategies were used for the deprotonation of the pro-ligand **3**. In the case of aluminum, the $AlMe_3$ precursor acts both as a strong basis (reaction between methylides and phenols releasing methane) and as a source of aluminum (Scheme 2). In the case of gallium, we opted for $GaCl_3$ as salt. Its use implies a preliminary step of deprotonation of the pro-ligand by addition of NaH in THF. The obtained solution was then added by filtering cannula into a solution of $GaCl_3$ in THF (Scheme 2). The expected complexes were obtained in good yields after purification by precipitation with a mixture dichloromethane/pentane (v/v, 1/4).

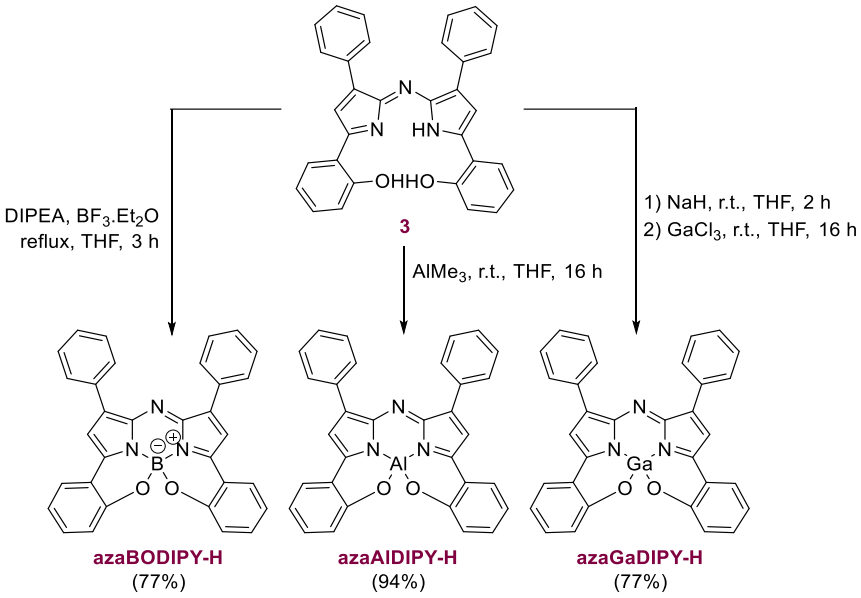

*Scheme 2: Synthesis of the **azaBODIPY-H** and azaMDIPY-H analogues (it has to be noted that a molecule of solvent – THF in these cases – completes the coordination sphere of Al(III) and Ga(III) as an "L" ligand).*

^{1}H-NMR analysis allows following easily the progress of the chelation of B, Al, and Ga. It has been found that all signals of the ligand are upfield shift in the case of the Al and Ga complexes, whereas it is not true or less significant in the case of boron. It is worth noting that the aza-BODIPY is red-brown in solution in DMSO, whereas the **azaAlDIPY-H** and **azaGaDIPY-H** complexes are green. Moreover, it appears that the aluminum and gallium complexes exhibit a good stability of at least two weeks in wet DMSO.

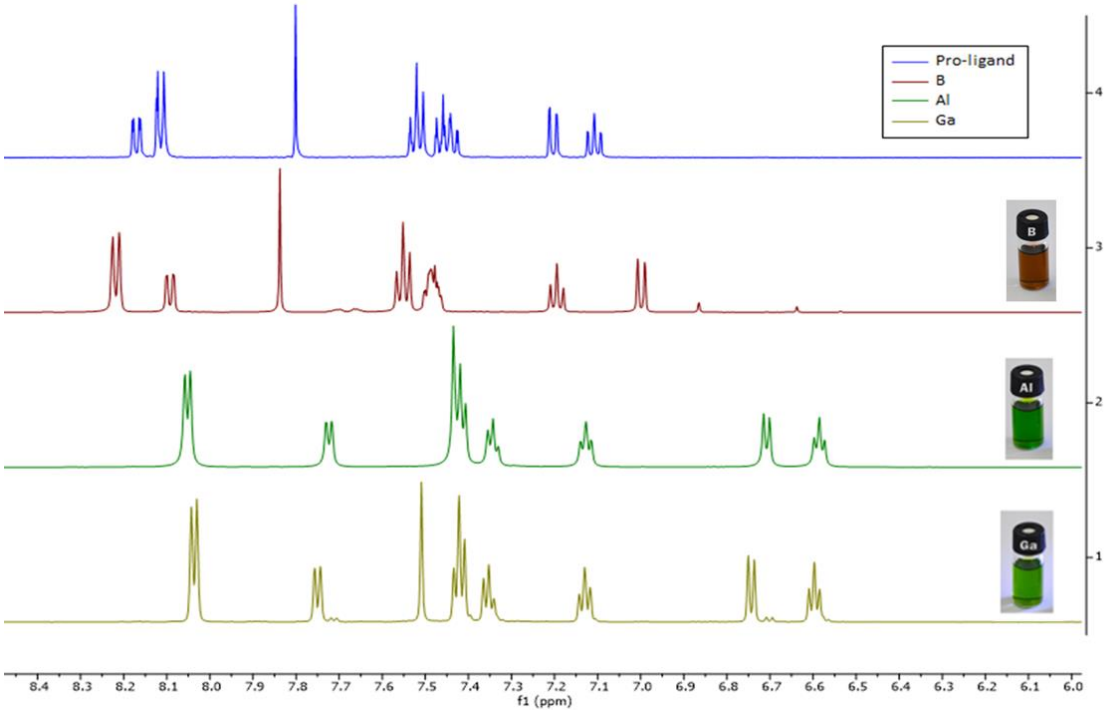

*Figure 2: 1H-NMR spectra of **3**, **azaBODIPY-H**, **azaAlDIPY-H**, and **azaGaDIPY-H** in DMSO-d_6 at 298 K.*

Single crystals were obtained by slow diffusion of pentane in a THF solution of **azaGaDIPY-H**. The structure of the THF adduct of **azaGaDIPY-H** was elucidated by X-ray diffraction. This structure reveals that the complex exists as a dimer bridged by one of the two phenate oxygen atoms of each ligand to form a four-membered Ga_2O_2 ring (Figure 3). The gallium is thus found in a O_h symmetry placed in the middle of an octahedron where both nitrogen atoms, N1 and N3, and both oxygen, O1 and O2, form the base of the coordination sphere (maximum plane deviation for O2 O1 N1 N3 Ga1 plane was found for O2 (0.147 Å)). The coordination sphere of the metal was completed by an oxygen atom O3 from a solvent molecule in apical position and an oxygen atom $O2^i$ from another ligand. These both octahedra share a common edge formed by oxygen atoms O2 and $O2^i$.

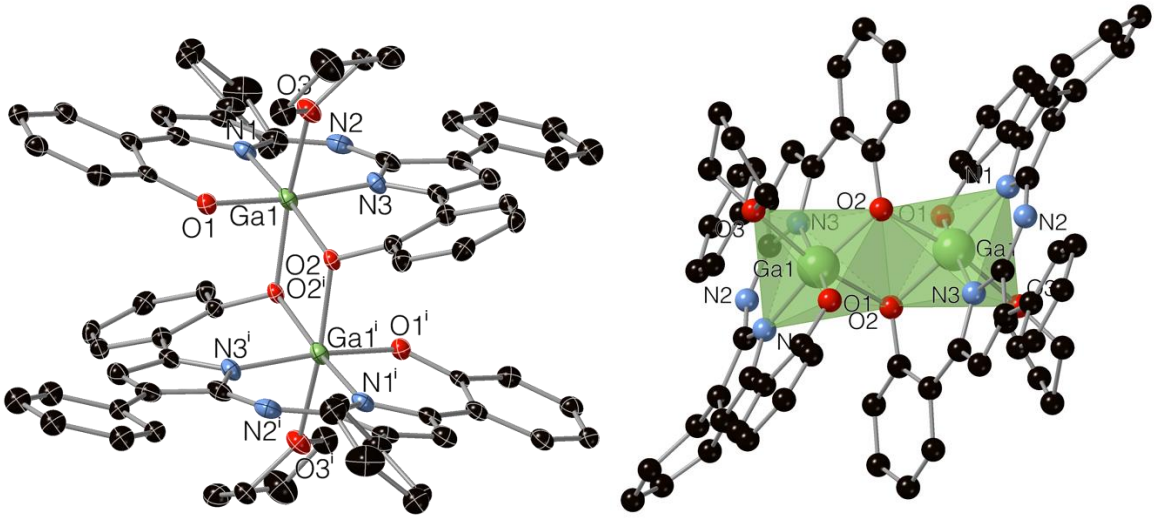

*Figure 3: on left: view of **azaGaDIPY-H** complex. Disordered parts and H atoms are omitted for clarity. Thermal ellipsoids are drawn at 50% probability plot. Symmetry operation used i = (1-x, 1-y, -z). Selected bond lengths (Å) and angles (°): Ga1-O1 =1.879(2), Ga1-O2i = 2.063(2), Ga1 - O2 = 1.962(2), Ga1-O3 = 2.219(2), Ga1 - N1 = 1.957(2), Ga1-N3 = 1.961(2), O1-Ga1-O2 = 90.15(8), O1-Ga1-O2i = 94.52(8), O1-Ga1-O3 = 83.76(8), O1-Ga1-N1 = 2.53(9), O1-Ga1-N3 = 171.16(9), O2-Ga1-Oi = 77.97(8), O2i -Ga1-O3 = 168.33(7), O2-Ga1-O3 = 90.47(7), N1-Ga1-O2 = 171.24(9), N1-Ga1-O2i = 93.50(8), N1-Ga1-O3 = 98.11(8), N1-Ga1-N3 = 89.46(10), N3-Ga1-O2 = 89.15(9), N3-Ga1-O2i = 93.95(8), N3-Ga1-O3 = 87.43(8). on right: view of both octahedron around Gallium.*

This structure is similar to that described by Nabeshima *et al.* in 2019 in the case of a GaDIPY.[40] The authors had shown that in the presence of pyridine, it was possible to obtain crystals of the mononuclear complex where two pyridines completed the coordination sphere at the apical position. In DMSO, this solvent molecule is exchanged and the adduct azaGaDIPY.DMSO should be formed (such an adduct can be seen on HR-MS analysis for **azaGaDIPY-OMe** and **azaAlDIPY-H**). Thus, taking in consideration the ^{1}H-NMR spectrum of **azaGaDIPY-H**, it is likely that the monometallic species is present in solution, especially in coordinating solvents. This was confirmed by a DOSY experiment performed in DMSO-d_6 (see supporting information S48-S50).

Following the successful synthesis of these complexes, we chose to synthesize other aza-DIPY ligands by varying the substituent in the *para* position of the aromatic rings to the north of the aza-DIPY. With this purpose, on the basis of Hammett's constant (σ),[41] we have chosen a rather electron-withdrawing substituent (Br, σ = 0.23), an electron-donating substituent (OMe, σ = -0.27) and a very electron-donating substituent (NMe_2, σ = -0.83). The synthesis of the aza-DIPY as well as the synthesis of the corresponding gallium (III) complexes were carried out following the same procedures presented previously (Scheme 3).

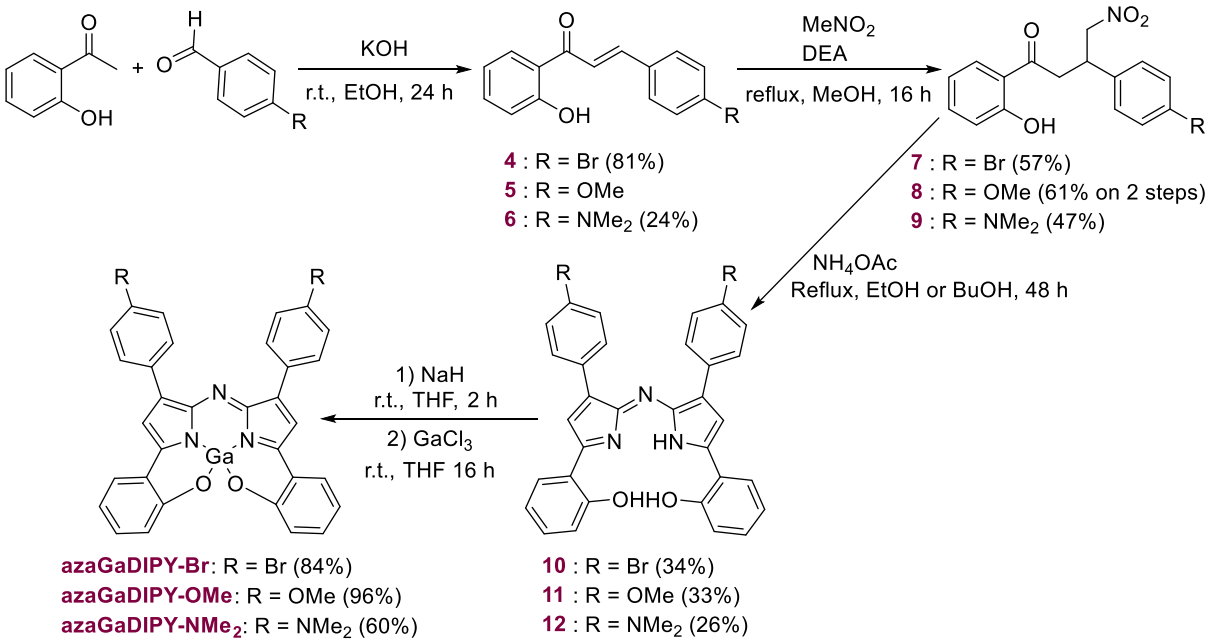

*Scheme 3: synthesis of Ga(III) complexes **azaGaDIPY-Br**, **azaGaDIPY-OMe**, and **azaGaDIPY-NMe$_2$**.*

Photophysical properties

The photophysical characterization including absorption, excitation, and emission spectra of the presented compounds was studied in a diluted DMSO solution. Additionally, the fluorescence quantum yield and the radiative lifetimes were measured to further describe the excited states of the cited compounds. The main photophysical properties are summarized in Table 1 and depicted in Figure 4.

Table 1: Summary of the main spectroscopic and photophysical data for all studied AzaMDIPY derivatives in diluted DMSO solution.

Compounds	$\lambda_{abs(max)}$ (nm)	ε (L.Mol^{-1}.cm^{-1})	λ_{em} (nm)	Φ_f	τ_{obs} (ns)	Δ_{SS} (cm^{-1})
azaBODIPY-H	728	52,000	756	0.28[a]	4.31	509
azaAlDIPY-H*	732	87,000	787	0.13[a]	2.39	955
azaGaDIPY-H*	728	81,000	782	0.11[a]	2.22	949
azaGaDIPY-Br*	744	32,000	802	0.08[a]	2.05	972
azaGaDIPY-OMe*	734	110,000	782	0.14[a], 0.17[b]	-	836
azaGaDIPY-NMe$_2$*	754	75,000	796	0.10[b]	-	700

a. Using "bismethoxy" azaBODIPY (Figure S1) as reference (Φ_F = 0.36 in chloroform) with λ_{exc} = 650 nm.[10,42]

b. Using IR 125 as reference (Φ_F = 0.132 in ethanol) with λ_{exc} = 680 nm.[43]

*for the calculation of epsilon of these complexes, one molecule of THF was added to the M of the complexes.

The absorption spectra of the parent **azaBODIPY-H** and the azaMDIPYs derivatives are comparable, with a main broad absorption band around 730 nm corresponding to the So → S_1 transition (Figure 4). By contrast, the molar absorptivity is higher for the Al and Ga analogues, as pointed out by TD-DFT calculations (*vide infra*). The emission spectra of the azaMDIPYs derivatives show a redshift of around 30 nm of the main fluorescence band in comparison to the analogue **azaBODIPY-H**, thus, indicating the direct effect of the metal substitution on the photophysical properties in agreement with the NMR results. Therefore, the Stoke's Shifts of the Al and Ga derivatives are much enhanced. Interestingly, the

fluorescence quantum yield of the metal analogues remains relatively high as for a NIR emitter. The same behavior was found in the case of the excited states lifetimes.

When moving to the substitution of the phenyl ring of the Ga analogue with either electron-withdrawing or electron-donating groups, the photophysical properties were very little modified, thus, suggesting that both HOMO and LUMO are little modified by the substituents and therefore, the energy gap almost maintained. This effect will be further studied by cyclovoltammetry. It is worth highlighting the relative high quantum yields measured for all derivatives independently of the substituents. These observations are interesting for the development of future fluorescent probes. It suggests that it would be possible to functionalize the molecule – e.g. adding a biovector - *via* one of these positions without significantly affecting the photophysical properties of the molecule.

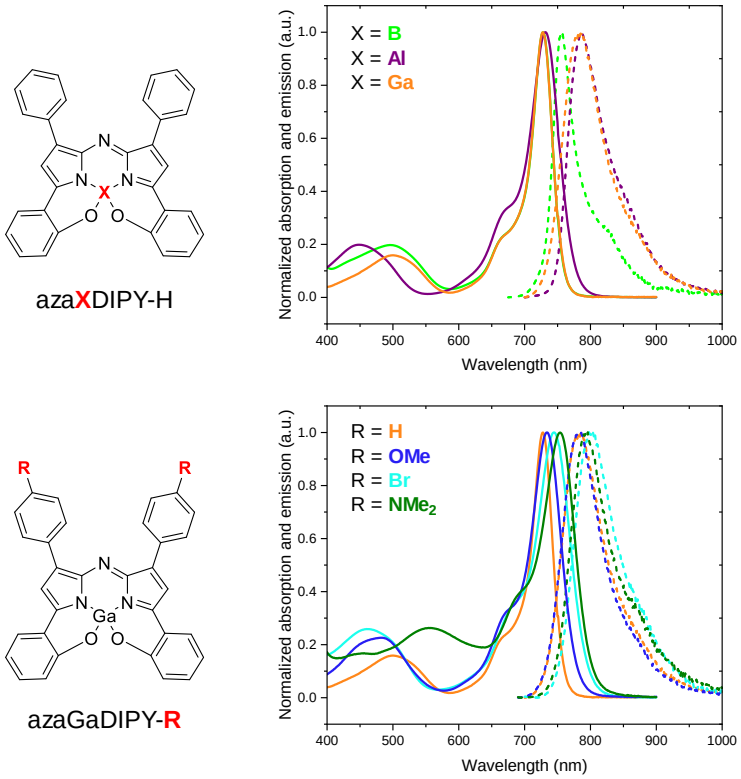

Figure 4. Absorption (full lines) and emission (dotted lines) spectra of the studied compounds.

(TD-)DFT calculations

To give more insights into the photophysical properties, (TD-)DFT calculations have been carried out on the **azaXDIPY-H** complexes (see computational details in experimental section). The ground state geometries of the **azaXDIPY-H** compounds mainly differ in the coordination of X (B/Al/Ga). The B center in **AzaBODIPY-H** is close to a tetrahedral configuration,[30] while the Al et Ga centers are midway between a tetrahedral and a plane square environment (see Figure S60 for a representation). In all three **azaXDIPY-H** compounds, the computed absorption profile is dominated by an intense S_0 -> S_1 excitation, corresponding to a π -> π^* electronic transition localized on the arms, with no contribution of the B/Al/Ga center. The emission is described by a very similar electronic transition, with the S_1 relaxed geometries showing very small reorganization of the molecule, in agreement with the small and similar Stokes shifts within the series (Figure 5).

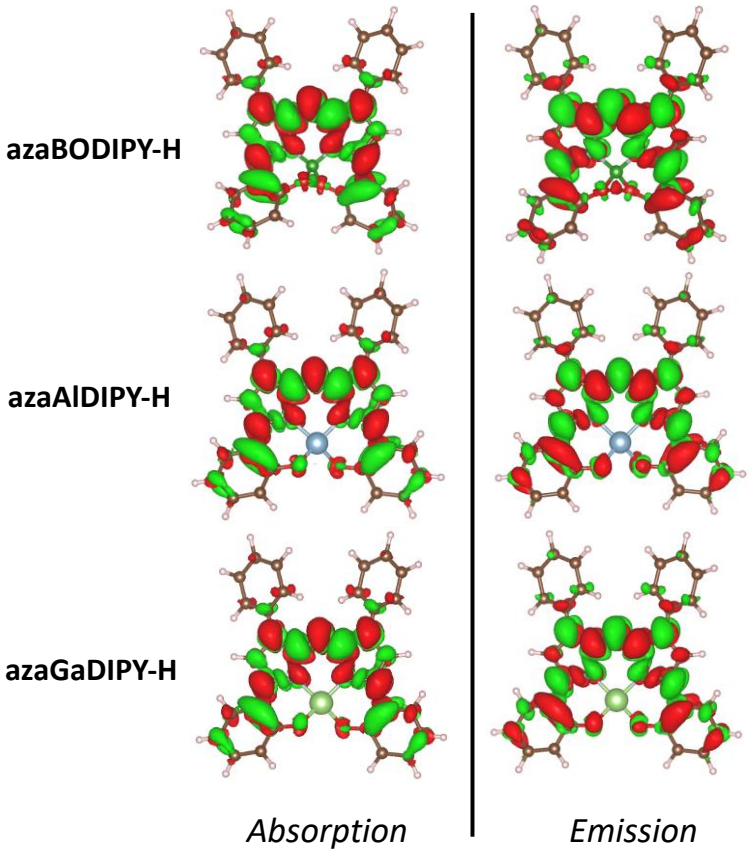

Figure 5: Density difference between the ground and excited state for absorption (left) and emission (right) (isovalue of 0.0005 au) for azaXDIPY-H compounds in DMSO. Red and green surfaces represent respectively a gain and a loss of electronic density.

To investigate the possible coordination of a solvent molecule on the metal center, the geometries of **azaX(DMSO)$_n$DIPY-H** molecules (n=1 or 2) have been relaxed, where the DMSO are explicitly placed on the axial positions and coordinate the metal through their oxygen atom (Figure S60). On the one hand, for **AzaBODIPY-H**, the presence of one DMSO strongly disturbs the binding situation of the boron center and leads to the de-coordination of one the O-Ph arm. In addition, no stable structure is found for **azaB(DMSO)$_2$DIPY-H**. The boron derivative is therefore considered as not being coordinated with additional DMSO in the following. One the other hand, both **azaAlDIPY-H** and **azaGaDIPY-H** molecules are predicted to be able to accept either one or two DMSO units as additional ligands on the metal center. The **azaAl(DMSO)DIPY-H** and **azaGa(DMSO)DIPY-H** exhibit a square-based pyramid like and the original pseudo plane square is only slightly disturbed. The **azaAl(DMSO)$_2$DIPY-H** and **azaGa(DMSO)$_2$DIPY-H** present an octahedral configuration.

Upon addition of the DMSO ligands on **azaAlDIPY-H** and **azaGaDIPY-H**, the computed absorption and emission profile show no clear change in the transition densities (Figure 6). Nevertheless, this results in a red-shift of the electronic transitions and an increase in their oscillator strengths, as detailed in Table 2. When comparing the measured absorption and emission characteristics to the computed ones, considering that one DMSO coordinates **azaAlDIPY-H** and **azaGaDIPY-H**, along with a DMSO-free **azaBODIPY-H** allows recovering the trends in the series. Indeed, only this situation leads to very similar absorption wavelengths for B, Al and Ga derivatives (648/643/648 nm respectively), with a greater oscillator strength (to correlate with a greater ε value) for the two latter**.** At the same time, this allows to retrieve the non-negligible red-shift of the emission of Al and Ga compounds (827/826 nm) compared to their boron counterpart (787 nm).

Table 2: Computed absorption and emission properties for azaXDIPY-H compounds in DMSO. See Computational Details section for additional information.

Compound	λ_{abs} (nm) / E_{abs} (eV)	f_{abs}	$states_{abs}$	λ_{em} (nm) / E_{em} (eV)	f_{em}	Δ_{SS} (cm^{-1})
azaBODIPY-H	648 / 1.91	0.56	S_1	787 / 1.58	0.73	2662
azaAlDIPY-H	626 / 1.98	0.78	S_1	780 / 1.59	0.92	3146
azaAl(DMSO)DIPY-H	643 /1.93	0.69	S_1	827 / 1.50	0.81	3468
azaAl(DMSO)$_2$DIPY-H	657 / 1.89	0.61	S_1	814 / 1.52	0.84	2984
azaGaDIPY-H	628 / 1.97	0.75	S_1	770 / 1.61	0.94	2904
azaGa(DMSO)DIPY-H	648 / 1.91	0.67	S_1	826 / 1.50	0.81	3307
azaGa(DMSO)$_2$DIPY-H	659 / 1.88	0.60	S_1	814 / 1.52	0.84	2904

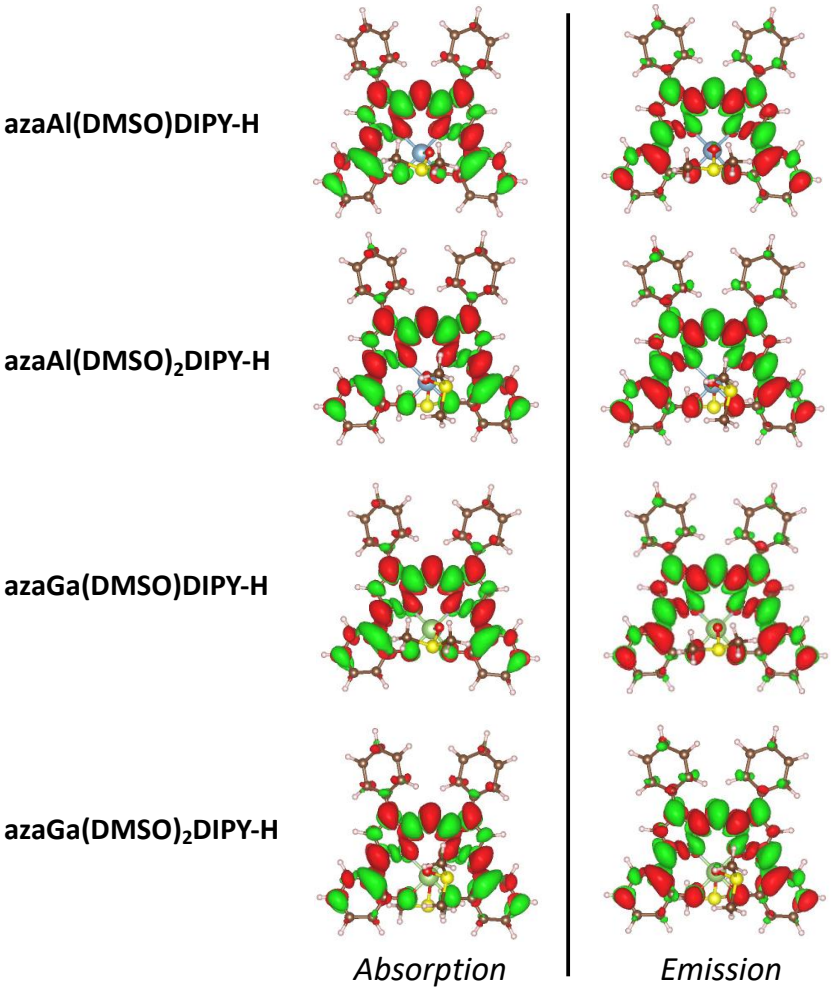

*Figure 6: Density difference between the ground and excited state for absorption (left) and emission (right) (isovalue of 0.0005 au) for **azaAl(DMSO)nDIPY-H** and **azaGa(DMSO)nDIPY-H** compounds (n=1, 2) in DMSO. Red and green surfaces represent respectively a gain and a loss of electronic density.*

Electrochemical characterization

The electrochemical signature of the B, Al and Ga complexes was investigated to better highlight the impact of the metal and of the substituents on the properties of the azaMDIPY complexes. These analyses were performed in DMF in the presence of tetra-*n*-butylammonium used as an electrolyte (0.1 M). All measurements were carried out under N_2 (glovebox) in a home-made three electrodes cell including an $AgNO_3$ (10^{-2}M in CH_3CN)/Ag reference electrode and a vitreous carbon disk (∅ = 3mm) as a working electrode. The potential values measured by cyclic voltammetry (CV) in these experimental conditions are collected in Table 3.

Table 3: Half wave and peak potential values (in Volts) measured by Cyclic Voltammetry (CV).

Entry	Compound	E^{3c}	E^{2c}	E^{1c}	E^{1a}	E^{2a}
1	azaAlDIPY-H	- 2.105 [a]	- 1.921 [a]	- 1.403 [a]	0.075 [b]	0.556 [a]
2	azaGaDIPY-H	-	- 1.890 [a]	- 1.310 [a]	0.169 [a]	0.292 [a]
3	azaBODIPY-H	-	- 1.555 [b]	- 0.740 [b]	0.674 [a]	-
4	azaGaDIPY-Br	-	- 1.783 [a]	- 1.244 [a]	0.189 [a]	0.016 [a]
5	azaGaDIPY-OMe	-	-1.983 [a]	- 1.331 [a]	0.107 [b]	0.561 [a]
6	azaGaDIPY-NMe_2	-	-	- 1.470 [a]	0.032 [b]	0.0271 [b]
7	azaDIPY-H	-	-1.515 [a]	-1.118 [a]	0.536 [a]	

Measured by CV at 1 × 10−3 M in DMF + TBAP (0.1 M), vitreous carbon working electrode Ø = 3 mm, 298 K, v = 0.1 V·s−1; Potential values are given in Volts *vs.* E_{ref}[Ag^+($AgNO_3$ 0.01 M in MeCN)/Ag]; [a] peak potential (irreversible waves); [b] half-wave potential values ($E_{1/2}$=(E_{pa}+E_{pc})/2

These key figures reveal that each compound undergo several oxidation and reduction processes within the accessible potential window. We first found that the CV curve of the free ligand exhibits one fully irreversible multi-electron oxidation wave and two irreversible reduction waves. The irreversibility of all the observed waves is moreover consistent with the existence of chemical steps coupled to the transfer of electrons most likely involving intra or inter molecular proton transfer between the ”acidic” and “basic” sites involved in the molecule.[44] One driving force for such proton-coupled electron transfer (PCET) is that the oxidation and reduction of the aza-DIPY **3** core strengthen the acidity of the phenol and the basicity of the “imine/amidine-type” subunits, respectively.

In agreement with this hypothesis, we found that the replacement of the three inner hydrogens by boron, gallium or aluminum has drastic effects on the shape and position of the observed waves (Figure 7 and Table 3). In the azaXDIPY-H series (with X = Al, B, Ga), each compound undergoes two consecutive one-electron reduction processes yielding successively [azaXDIPY-H]$^{\bullet-}$ and [azaXDIPY-H]$^{2-}$). Both reduction waves appear fully reversible at low scan rate (100 mV/s) when X = B only. The CV curves recorded in the same conditions with the gallium and aluminium analogues indeed feature two irreversible reduction waves demonstrating the poor stability of the intermediate radical anion [azaXDIPY-H]$^{\bullet-}$. The existence of a coupled chemical step is then readily demonstrated by the observation on an additional re-oxidation wave on the reverse scan attributed to the oxidation of the in-situ generated EC product (Figure 7). Further studies revealed that the reversibility of the first reduction wave can be recovered, and at the same time the intensity of the additional wave can be significantly decreased, upon shortening the time scale of the measurement from 100 to 500 mv/S. This is consistent with the conclusion that the chemical reaction coupled to the first reduction of

azaGaDIPY-H and **azaAlDIPY-H** is quite slow (see figures S53 and S54). Moreover, the fact that the additional reoxidation wave is not observed at the same potential on the CV curves recorded with **azaGaDIPY-H** and **azaAlDIPY-H** suggest that Ga and Al remains coordinated to the ligand in the final EC product.

On the anodic side, the electrochemical response varies quite significantly with the complexed atom. The reversible one electron oxidation wave observed with the Al complex indicates that the cation radical [**azaAlDIPY-H**]$^{+\bullet}$ is stable at the CV time scale. The Boron and Ga –based analogs were conversely found to be quite unstable, as evidenced by the observation of irreversible waves (**azaBODIPY-H**) and of quite complex signatures including many superimposed waves (**azaGaDIPY-H**). As a general statement, the relative position of the first oxidation and reduction waves recorded in the same conditions with **azaBODIPY-H**, **azaAlDIPY-H**, and **azaGaDIPY-H** were found to follow the electronegativity of the central atom, with $\chi_B > \chi_{Ga} > \chi_{Al}$. In agreement with this order, the reduction of the boron complex is observed at a much less negative potential value than the two other ones (E_{1c}[X=B] > E_{1c}[X=Ga] > E_{1c}[X=Al]) while the Al complex is easier to oxidize than the B and Ga complexes (E_{1a}[X=B] > E_{1a}[X=Ga] > E_{1a}[X=Al]). It should be mentioned that this simple interpretation seems relevant despite the irreversible character of most oxidation waves and despite the presence of additional ligands on the gallium atom.

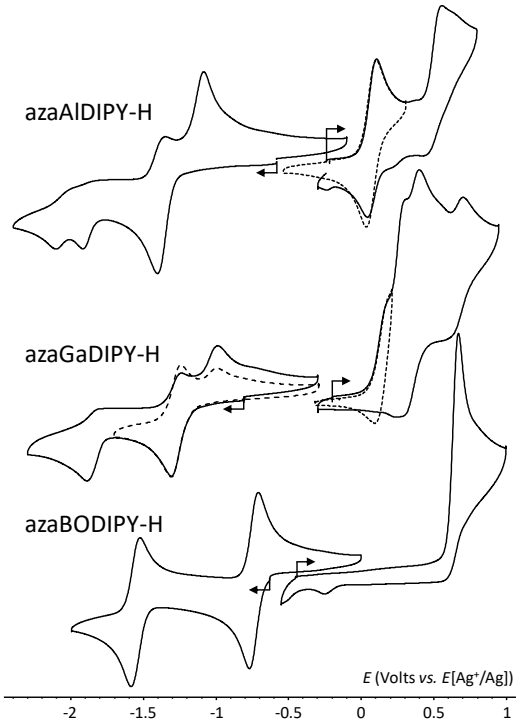

*Figure 7: Voltammetric curves of DMF (0.1M TBAP) solutions of **azaBODIPY-H**, **azaGaDIPY-H** and **azaAlDIPY-H** (v = 0.1 V s^{-1}, VC Φ = 3 mm,* E *(volt)* vs E_{ref} *[Ag$^+$(10^{-2} M)/Ag]).*

Further analyzes performed on the azaGaDIPY-R series, with R = H, Br, OMe and NMe_2, confirmed our assignment of the observed waves to ligand-centered electron transfers. As can be seen in Figure 8 and Table 3, replacing the *para*-hydrogen atom with electron-donating or electron-withdrawing substituents results in quite large shifts in the potential values associated to the first oxidation and reduction processes. These effects are best revealed by the shift of the first reversible reduction wave (Figure 8). Here again, the shift (amplitude, sign) is consistent with the electronic effect of the substituents, *i.e.* the Br atom facilitates the reduction, while the electron-donating groups like -OMe or -NMe_2 shift the reduction potential toward more negative values. It should be mentioned that the introduction of NMe_2 not only leads to the expected cathodic potential shift but also to an apparent splitting of the wave, which is most likely attributed to the instability of the reduced species.

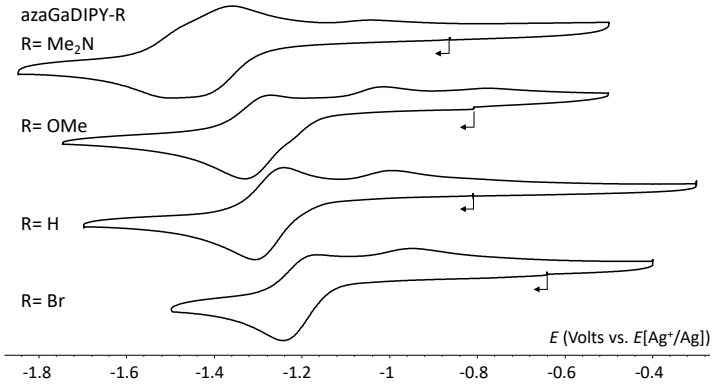

Figure 8: Voltammetric curves of DMF (0.1M TBAP) solutions of azaGaDIPY-R with R = Me_2N, OMe, H and Br (v = 0.1 V s^{-1}, VC Φ = 3 mm, E *(volt)* vs E_{ref} *[$Ag^+(10^{-2}$ M)/Ag]).*

On the anodic side, the CV curve recorded with **azaGaDIPY-OMe** exhibits similar features to that obtained with **azaGaDIPY-H**, with two successive one-electron oxidations observed in the [0-1] volt range (Figure 9). This "standard" signature contrasts with that obtained in the same conditions with the **azaGaDIPY-NMe_2** analog incorporating two redox-active dimethylaniline subunits. As can be seen in Figure 9, the CV curve obtained with **azaGaDIPY-NMe_2** displays at least three successive one-electron oxidation processes including two first one-electron reversible waves attributed to the oxidation of the aza-DIPY core. This specific pattern, observed only when R= NMe_2, make us propose that the dimethylaniline units are involved in the irreversible processes observed at E>0.5 V, a hypothesis which was finally confirmed by showing that the dimethylaniline subunits are oxidized in the same experimental conditions at about 0.45 V (Figure S55).

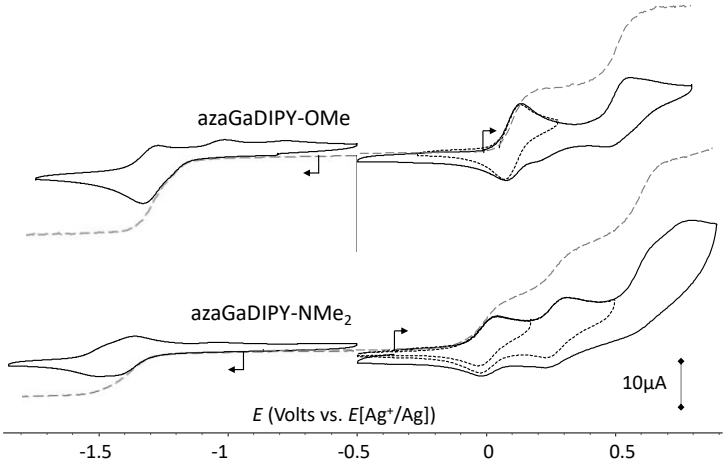

*Figure 9: Voltamperometric curves of DMF solutions of **azaGaDIPY-OMe** and **azaGaDIPY-NMe_2** (1x10-3 M + 0.1M in TBAP) recorded at a vitreous carbon working electrode (full line, Ø = 3 mm, 0.1 V.s-1) and at a rotating disk electrode (dashed lines, Ø = 3 mm, 0.01 V.s-1, 500 rd.min-1).*

Spectroelectrochemical (SEC) analyses have then been conducted with **azaGaDIPY-OMe** to gain further insights into the stability and into the spectroscopic signature of the oxidized and reduced species. Those measurements were carried out upon collecting time-resolved UV/Vis spectra during the electrochemical reduction/oxidation of **azaGaDIPY-OMe** carried out at a platinum gauze electrode placed in a thin layer SEC cell (0.5 mm). The one-electron oxidation of **azaGaDIPY-OMe** led to a large decrease in the intensity of the absorption centered at 729 nm at the expense of two less intense signals developing at λ_{max} = 850 and 982 nm. This conversion was found to be chemically reversible, as proved by the fact that the initial absorption band could be recovered by subsequent reduction of the solution. Observation of a clean isobestic points at 594 and 768 nm also confirmed that no secondary

reactions occurred over the time scale of the experiment. Similar measurements were carried out focusing on the first reduction wave. Setting the electrode potential at -1.5 V led to a large decrease in the intensity of the initial waves at λ_{max} =729 and 476 nm at the expense of a weak band at 870 nm and of a more intense one at 400 nm. Here again, these changes were seen to proceed through at least two isosbestic points at 436 and 813 nm. Most surprisingly, we found that the starting molecule **azaGaDIPY-OMe** can be fullly recovered after reoxidation of the sample, which includes the reoxidation of [**azaGaDIPY-OMe**]$^{\bullet-}$ (* in Figure 10) followed by the oxidation of the side product (** in Figure 10). These results thus demonstrate that the transformation undergone by [**azaGaDIPY-OMe**]$^{\bullet-}$ is reversible at the SEC time scale.

Taken together, these (spectro)electrochemical studies demonstrate the stability of the reduced and oxidized forms of **azaGaDIPY-OMe**, which is very promising from the perspective of *in vivo* applications.

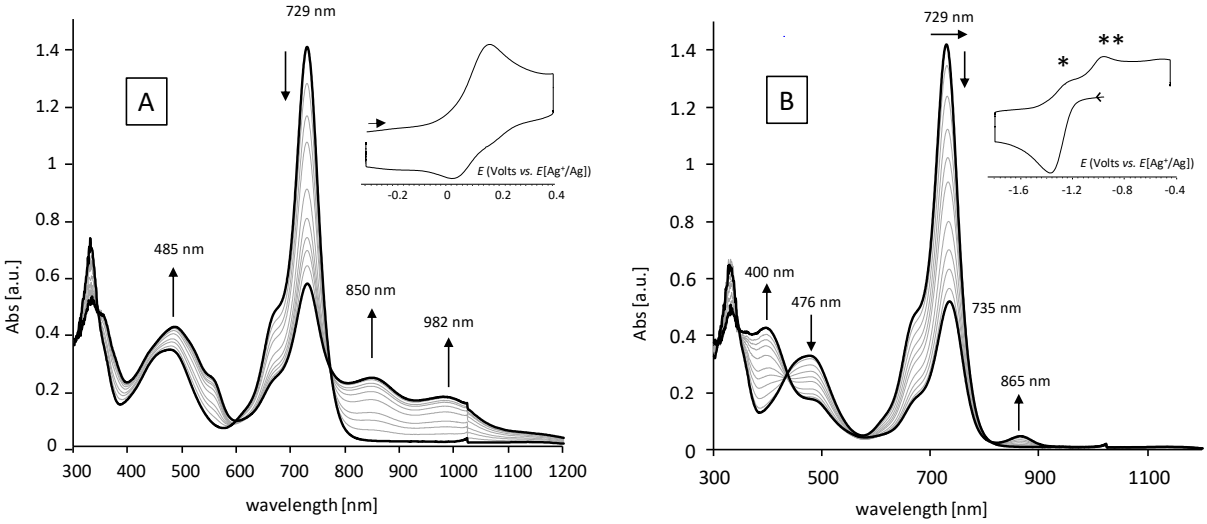

*Figure 10: UV-vis spectra recorded during the oxidation (A) and reduction (B) of **azaGaDIPY-OMe** in DMF (0.1M TBAP) at a platinum gauze working electrode (l = 0.5 mm, v = 10mV/s). The current potential curves recorded at the working electrode are shown as insets.*

Conclusion

A series of N_2O_2-azaDIPY-based complexes of group 13 elements was firstly synthesized and characterized. This study show the potential of the aza-DIPY-biphenate ligands to design and obtain a new class of NIR-emitting fluorophores. The replacement of the boron by aluminum or gallium enable to redshift the emission of fluorescence of 30 nm in the NIR, while keeping a good brightness. One complex even displays a tail of its emission in the NIR-II area. This increase of the maximum emission wavelength is likely to be due to the ability of the metallic center to coordinate an additional molecule (e.g. coordinating solvent), which induces an increased planarity of the azaMDIPY core, more than the nature of the metal. The different complexes appeared to be air stable, even in solution, and did not release their metal ion even when reduced or oxidized. Their redox properties can be easily tuned by introducing electron-withdrawing or electron-donating groups on the backbone of the aza-DIPY. Such a modification of the azaMDIPY substituents leads to a redshift of the maximum absorption and emission wavelengths in the case of the introduction an electron-withdrawing group and in the case of the introduction of a strong electron-donating group. All these results let think that this new class of compounds will be promising for the development of innovative fluorescent probes for medical imaging or other applications.

Experimental section

Materials

Reactions were carried out in analytical reagent grade solvents from Carlo Erba under normal atmosphere. Dry solvents were non-stabilized, purchased from Carlo Erba and dried using a MB-SPS-800 (MBraun™) or PureSolv-MD-5 (Inert™). All reagents were purchased from SigmaAldrich™, Thermo Fisher Scientific™ or ACROS Organics™ and used as received without further purification. Reactions were monitored by thin-layer chromatography and NMR ^{1}H. Analytical thin-layer chromatography was performed with Merck 60 F254 silica gel (precoated sheets, 0.2 mm thick). Column chromatography was carried out using silica gel (SigmaAldrich, 40-63 µm 230-400 mesh 60Å).

Instrumentation

NMR Spectroscopy:

(^{1}H, ^{13}C, ^{11}B) were recorded at 298 K on Bruker spectrometers Avance Neo 500 MHz equipped with a 5 mm BBOF iProbe and Avance III HD 600 MHz equipped with a 5 mm BBOF N_2 cryoprobe. NMR spectroscopy chemical shifts are quoted in parts per million (δ) relative to TMS (for ^{1}H, ^{13}C), BF_3*Et_2O (for ^{11}B), calibration was made by using residual signals of the partially deuterated solvent summarized in 2010 by Fulmer et al.[45] For all other nuclei, SR value obtained after zero-calibration of the corresponding reference was applied.

Mass Spectrometry:

High-resolution mass spectrometry analyses were recorded on a LTQ Orbitrap XL mass spectrometer (Thermo Scientific) equipped with an electrospray ionization source (HESI 2). The following source parameters were used if no further specification is mentioned:

Heater Temperature: 50 °C
Gas Flow: Sheath 15 / Aux 10 / Sweep 0
Spray Voltage: 4 kV
Capillary Temperature: 275 °C
Capillary Voltage: 22 V
Resolution (m/z = 400): 60 000

Typical conditioning: A stock solution of the analyte was prepared by dissolving 1 mg of the analyte in 1 mL of a HPLC-grade solvent MeOH or in RPE-grade DMSO. For small molecules (MW < 1000 Da) a 1/100 dilution was performed using 10.0 µL of the stock solution completed to 1.0 mL by a HPLC-grade solvent. For high weight molecules (MW> 1000 Da) a 1/10 dilution was performed using 100.0 µL of the stock solution completed to 1.0 mL by a HPLC-grade solvent.

The 10^{-5} M resulting solution of the analyte was then directly infused into the spectrometer using a 500 µL syringe. The system was rinsed three times between two consecutive analyses with 500 µL of HPLC grade water and/or MeOH. Mass calibration in the 100-2000 Da mass range was operated using the commercially available Pierce LTQ ESI Positive/Negative ion Calibration solutions (Thermofisher Scientific ref 88322/88324).

NMR and mass-analyses were performed at the “Plateforme d’Analyse Chimique et de Synthèse Moléculaire de l’Université de Bourgogne” (PACSMUB).

Analytical HPLC:

HPLC-MS analyses were obtained on a on a ThermoFisher Vanquish instrument (pump + autosampler at 20 °C + column oven at 25 °C) equipped with a UV-visible DAD and ISQ-EM single quadrupole mass spectrometer. RP-HPLC-fluorescence (Phenomenex Kinetex C_{18} column, 2.6 µm, 2.1 × 50 mm) with MeCN + 0.1% formic acid (B) and H_20 + 0.1% formic acid (A) as eluents [5% B (2 min) followed by linear gradient from 5% to 100% (5 min) of B, then 100% B (1.55 min)] at a flow rate of 0.5 mL/min. UV-visible detection was achieved at 214, 254, 280 and 650 nm (+ diode array detection in the range of 220-500 nm). Low resolution ESI-MS detection in the positive/negative mode (full scan, 100-2000 a.m.u., data type: centroid, source CID voltage: 20 V, vaporizer temperature: 282 °C, ion transfer tube temperature: 300°C, source voltage positive ions: 3 kV, source voltage negative ions: -2 kV and sheet gas pressure: 49.9 psig.

Photophysical studies:

UV-Visible absorption spectra of aza-MDIPY (B, Al, Ga) were recorded on a Varian Cary 50 scan (single-beam). Data are reported as absorption maximum wavelength ([λ_{max}] = nm) and molar absorption coefficient at the absorption maximum wavelength ([ε] = $M^{-1}.cm^{-1}$). The steady-state fluorescence emission spectra of aza-MDIPY were obtained using a HORIBA Jobin Yvon fluorolog spectrofluorometer (software FluoEssence). The steady-state fluorescence emission spectra of aza-MDIPY were obtained using a HORIBA Jobin Yvon Fluorolog spectrofluorometer (software FluorEssence). All fluorescence spectra were corrected for apparatus response. Quartz cuvettes (1.5 mL) with an optical path of 1 cm were used. The sample concentrations were chosen to obtain a maximum absorbance between 0.3 and 1.0 for UV spectra and between 0.035 and 0.1 at excitation wavelength for quantum yield measurements. Relative quantum yields were obtained by comparing the areas under the corrected emission spectrum. All measurements were performed in DMSO (Sigma Aldrich, spectroscopic grade ≥ 99.9 %) and DCM at 298 K. "bismethoxy" AzaBODIPY (see ESI Figure S1) (Φ = 0.36 in $CHCl_3$, λ_{ex} = 670 nm)[42] and IR 125 (Φ_F = 0.132 in ethanol)[43] with λ_{exc} = 680 nm was was used as the standard.

Computational details

All (TD-)DFT calculations presented in this work have been obtained with the Gaussian16 software,[46] using the PBE0[47] functional and a 6-311+G(d,p) basis set. The ground and excited state geometry optimizations of the compounds were followed by a frequencies calculation to identify the structures as minima of energy. Absorption profiles were obtained by computing the 15 first electronic excitations, and the emission energies were deduced form the first excitation at the excited state relaxed geometry. In all steps, solvent effects (dimethylsulfoxyde) were included through a Polarizable Continuum Model (PCM),[48] and the Linear-Response formalism of PCM was used for TD-DFT calculations.

Synthetic procedures

*The compounds **1**-**9**, **11**, **12**, and **azaBODIPY-H** were synthesized according to a modified reported procedure (NMR data are in agreement with literature, see details in ESI).*[49,50] *Concerning AzaMDIPY complexes, "yield*" means that we have considered that one molecule of THF is included in the molecular mass of the complex, when we calculated the yield.*

Pro-ligand 10:

Compound **6** (7.56 g, 20.8 mmol, 1 eq) was dissolved in 130 mL of EtOH in a 500 mL round bottom flask. NH_4OAc (43.18 g, 560.3 mmol, 27 eq) was added and the suspension refluxed during 2 days. Upon completion, the solvents were evaporated to the quarter of the initial volume. The supernatant

was filtered and the powder was washed with cold MeOH until the filtrate became blue and the solid residue exhibits a clean glossy surface. The solid was transferred into a round bottom flask and dried under vacuum to isolate the corresponding aza-dipyrromethene **10** as a green powder (2.28 g, 34 % yield).

^{1}H NMR (500 MHz, 298 K, DMSO-d_6) δ (ppm) = 7.02-7.05 (m, 2H), 7.12 (d, ^3J = 8.2 Hz, 2H), 7.36-7.38 (m, 2H), 7.66 (d, ^3J = 8.2 Hz, 4H), 7.75 (s, 2H), 7.96 (d, ^3J = 8.2 Hz, 4H), 8.02 (d, ^3J = 8.2 Hz, 2H). **^{13}C NMR** (125 MHz, 298 K, DMSO-d_6) δ (ppm) = 117.0, 117.2, 117.4, 120.2, 121.6, 128.9, 130.8, 131.3, 132.0, 132.6, 139.4, 146.1, 154.7, 157.4. **HR-MS** (ESI): *m/z* calculated for $C_{32}H_{21}Br_2N_3NaO_2^+$[M+Na]$^+$ 661.98723 Da, found 661.98613 Da.

AzaAlDIPY-H:

In the glovebox**, 3** (48 mg, 0.10 mmol, 1 eq) was dissolved in 3 mL of dry THF in a Schlenk tube. $AlMe_3$ (50 µL, 0.10 mmol, 1 eq) was added and the blue mixture turned to brown. The reaction mixture was stirred overnight under argon at room temperature and turned green. The crude product was evaporated to dryness, precipitated upon the addition of pentane, and the supernatant was removed. Pentane was added again and the supernatant removed (this operation was repeated three times). The resulting solid was then transferred into a round bottom flask and dried under vacuum to isolate the corresponding **AzaAlDIPY-H** as a black crystalline solid (47 mg, 81% yield*).

^{1}H NMR (600 MHz, 298 K, DMSO-d_6) δ (ppm) = 6.56-6.58 (m, 2H), 6.70 (d, ^3J = 8.2 Hz, 2H), 7.10-7.17 (m, 2H), 7.32-7.35 (m, 2H), 7.40-7.43 (m, 6H), 7.72 (d, ^3J = 7.8 Hz, 2H), 8.04 (d, ^3J = 7.6 Hz, 4H). **^{13}C NMR** (150 MHz, 298 K, DMSO-d_6) δ (ppm) = 114.9, 115.3, 119.1, 121.1, 127.4, 128.1, 128.1, 128.9, 131.7, 134.2, 140.4, 147.1, 156.6, 163.9. **HR-MS** in DMSO (ESI): *m/z* calculated for $C_{34}H_{26}AlN_3NaO_3S^+$ [M+DMSO+Na]$^+$ 606.14025 Da, found 606.14106 Da. **LC-MS**: Rt = 4.98 min.

AzaGaDIPY-H:

In the glovebox, compound **3** (40 mg, 0.08 mmol, 1 eq) and NaH (10 mg, 0.42 mmol, 5.2 eq) were dissolved in 2 mL of dry THF in a Schlenk tube. The initially blue solution turned into green and the reaction was stirred under argon at room temperature during 1 h. In the glovebox, $GaCl_3$ (15 mg, 0.08 mmol, 1 eq) was dissolved in 2 mL of dry THF in another Schlenk tube. The deprotonated ligand was then added using a filtering cannula into the $GaCl_3$ solution. The reaction mixture was stirred at room temperature during 2 h. The crude product was evaporated to dryness and solubilized with DCM. The resulting solution was filtered over celite to remove NaCl and evaporated to dryness. The compound was precipitated upon the addition of pentane and the supernatant was removed (this operation was repeated three time). The resulting solid was transferred into a round bottom flask and dried under vacuum to isolate the corresponding **AzaGaDIPY-H** as a green solid (36 mg, 73% yield*).

^{1}H NMR (600 MHz, 298 K, DMSO-d_6) δ (ppm) = 6.58-6.61 (m, 2H), 6.74 (d, ^3J = 8.2 Hz, 2H), 7.12-7.14 (m, 2H), 7.34-7.36 (m, 2H), 7.41-7.43 (m, 4H), 7.51 (s, 2H), 7.75 (d, ^3J = 8.2 Hz, 2H), 8.04 (d, ^3J = 7.6 Hz, 4H). **^{13}C NMR** (150 MHz, 298 K, DMSO-d_6) δ (ppm) = 115.1, 115.6, 117.7, 122.0, 127.7, 128.2, 128.7 128.9 , 131.7, 133.9, 140.5, 146.4, 157.2, 165.9. **HR-MS** (ESI): *m/z* calculated for $C_{32}H_{20}GaN_3NaO_2^+$ [M+Na]$^+$ 570.07035 Da, found 570.07200 Da. **LC-MS**: Rt = 5.21 min

AzaGaDIPY-Br:

In the glovebox, compound **10** (40 mg, 0.06 mmol, 1 eq) and NaH (10 mg, 0.41 mmol, 7 eq) were dissolved in 2 mL of dry THF in a Schlenk tube. The initially blue solution turned into green and the reaction stirred under argon at room temperature during 1 h. In the glovebox, $GaCl_3$ (11 mg, 0.06 mmol, 1 eq) was dissolved in 2 mL of dry THF in another Schlenk tube. Then, the deprotonated ligand

was added using a filtered cannula into the $GaCl_3$ solution. The reaction was stirred at room temperature during 2 h. The crude was evaporated to dryness and solubilized with DCM. The solution was filtered over celite to remove NaCl and evaporated to dryness. The compound was precipitated upon the addition of pentane and the supernatant was removed (this operation was repeated three time and then). The resulting solid was transferred into a round bottom flask and dried under vacuum to isolate the corresponding **AzaGaDIPY-Br** as a black powder (40 mg, 82% yield*).

^{1}H NMR (600 MHz, 298 K, DMSO-d_6) δ (ppm) = 6.58 (m, 2H, H_k), 6.74 (d, ^3J = 8.3 Hz, 2H), 7.12-7.15 (m, 2H), 7.56 (s, 2H), 7.63 (d, ^3J = 8.2 Hz, 4H), 7.74 (d, ^3J = 8.3 Hz, 2H), 7.96 (d, ^3J = 8.2 Hz, 4H). **^{13}C NMR** (150 MHz, 298 K, DMSO-d_6) δ (ppm) = 116.0, 116.1, 118.0, 121.6, 122.5, 129.2, 131.2, 131.6, 132.4, 133.5, 139.6, 146.8, 157.8, 166.4. **HR-MS** (ESI): *m/z* calculated for $C_{32}H_{18}GaBr_2N_3NaO_2^+$ $[M+Na]^+$ 727.88933 Da, found 727.89069 Da. **LC-MS**: Rt = 5.83 min

AzaGaDIPY-OMe:

In the glovebox, compound **11** (100 mg, 184 µmol, 1 eq) and NaH (22 mg, 920 µmol, 5 eq) were dissolved in 10 mL of dry THF in a Schlenk tube. The initially blue solution turned into green and the reaction was stirred under argon at room temperature during 1 h. In the glovebox, $GaCl_3$ (32 mg, 180 µmol, 1 eq) was dissolved in 2 mL of dry THF in an another Schlenk tube. Then, the deprotonated ligand was cannulated using a filtering cannula into the $GaCl_3$ solution. The reaction was stirred at room temperature during 30 min. The crude product was evaporated to dryness and solubilized with DCM. The solution was filtering over celite to remove NaCl and evaporated to dryness. The compound was precipitated upon the addition of pentane and the supernatant was removed (this operation was repeated three time). The resulting solid was transferred into a round bottom flask and dried under vacuum to isolate the corresponding **AzaGaDIPY-OMe** as a dark purple solid (107 mg, 85% yield*).

^{1}H NMR (500 MHz, 298 K, DMSO-d_6) δ (ppm) = 3.84 (s, 6H), 6.58 (ddd, ^3J = 8.0 Hz, ^3J = 6.9 Hz, ^3J = 1.3 Hz, 2H), 6.73 (dd, ^3J = 8.4 Hz, ^4J = 1.3 Hz, 2H), 7.00 (d, ^3J = 8.8 Hz, 4H), 7.11 (ddd, ^3J = 8.4 Hz, ^3J = 6.9 Hz, ^4J = 1.7 Hz, 2H), 7.40 (s, 2H), 7.73 (dd, ^3J = 8.0 Hz, ^4J = 1.7 Hz, 2H), 8.00 (d, ^3J = 8.8 Hz, 4H). **^{13}C NMR** (125 MHz, 298 K, DMSO-d_6) δ (ppm) = 55.2, 113.5, 113.7, 115.4, 117.8, 121.8, 126.6, 128.6, 130.2, 131.5, 140.3, 146.2, 156.9, 159.1, 165.8. **HR-MS** in DMSO (ESI): *m/z* calculated for $C_{36}H_{30}N_3O_5S$ $[M+DMSO]^+$ 685.11620 Da, found 685.11876 Da. **LC-MS**: Rt = 5.16 min.

AzaGaDIPY-NMe$_2$:

In the glovebox, compound **12** (100 mg, 176 µmol, 1 eq) and NaH (21 mg, 880 µmol, 5 eq) were dissolved in 10 mL of dry THF in a Schlenk tube. The initially blue solution turned into purple and gradually to green and the reaction was stirred under argon at room temperature during 1 h. In the glovebox, $GaCl_3$ (31 mg, 176 µmol, 1 eq) was dissolved in 2 mL of dry THF in another Schlenck tube. Then, the deprotonated ligand was cannulated using a filtered cannula into the $GaCl_3$ solution. The reaction was stirred at room temperature during 30 min. The solution was filtered over celite to remove NaCl and evaporated to dryness. The compound was precipitated upon the addition of pentane and the supernatant was removed (this operation was repeated three time). The solid was transferred into a round bottom flask and dried under vacuum to isolate the corresponding **AzaGaDIPY-NMe$_2$** as a dark purple solid (68 mg, 55% yield*).

^{1}H NMR (500 MHz, 298 K, DMSO-d_6) δ (ppm) = 3.00 (s, 12H), 6.57-6.60 (m, 2H), 6.69-6.71 (m, 2H), 6.77 (d, ^3J = 8.3 Hz, 4H), 7.07-7.10 (m, 2H), 7.26 (s, 2H), 7.70 (d, ^3J = 8.0 Hz, 2H), 7.96 (d, ^3J = 8.3 Hz, 4H). **^{13}C NMR** (125 MHz, 298 K, DMSO-d_6) δ (ppm) = 40.1, 111.3, 111.7, 115.2, 118.0, 121.8, 122.1, 128.1, 129.9, 131.1, 143.3, 146.6, 149.8, 154.9. **LC-MS:** Rt = 5.07 min

Crystallograhy

All experimental data procedure and refinement are detailed in Supplementary Information. Data **CCDC-2178000** contain the supplementary crystallographic data for this paper. These data can be obtained free of charge from The Cambridge Crystallographic Data Centre via www.ccdc.cam.ac.uk/data_request/cif

Acknowledgement

The Ministère de l'Enseignement Supérieur et de la Recherche, the Centre National de la Recherche Scientifique (CNRS), the Conseil Régional de Bourgogne (WT's PhD ICE grant), and the French Research National Agency (ANR) *via* project JCJC ''SPID" ANR-16-CE07-0020, JCJC "WazaBY" ANR-18-CE18-0012, and PRC "MAP" ANR-21-CE07-0025 are gratefully acknowledged. This work is part of the projects ''Pharmacoimagerie et agents théranostiques" et ''Chimie durable, environnement et agroalimentaire" supported by the Université de Bourgogne and the Conseil Régional de Bourgogne through the Plan d'Actions Régional pour l'Innovation (PARI) and the European Union through the PO FEDER-FSE Bourgogne 2014/2020 programs. We thank the Conseil Régional de Bourgogne Franche-Comté for its support via the project ANER "AZTHEC". FrenchBIC, GDR MAPYRO, and GDR AIM are acknowledged for fruitful discussion. B.L.G. and A.F. thank the French GENCI/IDRIS-CINES centers for high-performance computing resources. Ms M.-J. Penouilh and Mr. Q. Bonnin are gratefully acknowledged for HR-MS analysis, and Dr M. Picquet for NMR analyses. The authors would like to thank Dr V. Comte-Candas for her technical support.

References

(1) Pliquett, J.; Dubois, A.; Racoeur, C.; Mabrouk, N.; Amor, S.; Lescure, R.; Bettaïeb, A.; Collin, B.; Bernhard, C.; Denat, F.; Bellaye, P. S.; Paul, C.; Bodio, E.; Goze, C. A Promising Family of Fluorescent Water-Soluble Aza-BODIPY Dyes for *in Vivo* Molecular Imaging. *Bioconjug. Chem.* **2019**, *30* (4), 1061–1066. https://doi.org/10.1021/acs.bioconjchem.8b00795.

(2) Ge, Y.; O'Shea, D. F. Azadipyrromethenes: From Traditional Dye Chemistry to Leading Edge Applications. *Chem. Soc. Rev.* **2016**, *45* (14), 3846–3864. https://doi.org/10.1039/C6CS00200E.

(3) Shi, Z.; Han, X.; Hu, W.; Bai, H.; Peng, B.; Ji, L.; Fan, Q.; Li, L.; Huang, W. Bioapplications of Small Molecule Aza-BODIPY: From Rational Structural Design to *in Vivo* Investigations. *Chem. Soc. Rev.* **2020**, *49* (21), 7533–7567. https://doi.org/10.1039/D0CS00234H.

(4) Loudet, A.; Burgess, K. BODIPY Dyes and Their Derivatives: Syntheses and Spectroscopic Properties. *Chem. Rev.* **2007**, *107* (11), 4891–4932. https://doi.org/10.1021/cr078381n.

(5) Frangioni, J. In Vivo Near-Infrared Fluorescence Imaging. *Curr. Opin. Chem. Biol.* **2003**, *7* (5), 626–634. https://doi.org/10.1016/j.cbpa.2003.08.007.

(6) Carr, J. A.; Franke, D.; Caram, J. R.; Perkinson, C. F.; Saif, M.; Askoxylakis, V.; Datta, M.; Fukumura, D.; Jain, R. K.; Bawendi, M. G.; Bruns, O. T. Shortwave Infrared Fluorescence Imaging with the Clinically Approved Near-Infrared Dye Indocyanine Green. *Proc. Natl. Acad. Sci.* **2018**, *115* (17), 4465–4470. https://doi.org/10.1073/pnas.1718917115.

(7) Hong, G.; Antaris, A. L.; Dai, H. Near-Infrared Fluorophores for Biomedical Imaging. *Nat. Biomed. Eng.* **2017**, *1* (1), 0010. https://doi.org/10.1038/s41551-016-0010.

(8) Wang, S.; Li, B.; Zhang, F. Molecular Fluorophores for Deep-Tissue Bioimaging. *ACS Cent. Sci.* **2020**, *6* (8), 1302–1316. https://doi.org/10.1021/acscentsci.0c00544.

(9) Wu, D.; Xue, D.; Zhou, J.; Wang, Y.; Feng, Z.; Xu, J.; Lin, H.; Qian, J.; Cai, X. Extrahepatic Cholangiography in Near-Infrared II Window with the Clinically Approved Fluorescence Agent Indocyanine Green: A Promising Imaging Technology for Intraoperative Diagnosis. *Theranostics* **2020**, *10* (8), 3636–3651. https://doi.org/10.7150/thno.41127.

(10) Killoran, J.; Allen, L.; Gallagher, J. F.; Gallagher, W. M.; O'Shea, D. F. Synthesis of BF $_2$ Chelates of Tetraarylazadipyrromethenes and Evidence for Their Photodynamic Therapeutic Behaviour. *Chem Commun* **2002**, No. 17, 1862–1863. https://doi.org/10.1039/B204317C.
(11) Godard, A.; Kalot, G.; Pliquett, J.; Busser, B.; Le Guével, X.; Wegner, K. D.; Resch-Genger, U.; Rousselin, Y.; Coll, J.-L.; Denat, F.; Bodio, E.; Goze, C.; Sancey, L. Water-Soluble Aza-BODIPYs: Biocompatible Organic Dyes for High Contrast *In Vivo* NIR-II Imaging. *Bioconjug. Chem.* **2020**, *31* (4), 1088–1092. https://doi.org/10.1021/acs.bioconjchem.0c00175.
(12) Lim, H.; Seo, S.; Pascal, S.; Bellier, Q.; Rigaut, S.; Park, C.; Shin, H.; Maury, O.; Andraud, C.; Kim, E. NIR Electrofluorochromic Properties of Aza-Boron-Dipyrromethene Dyes. *Sci. Rep.* **2016**, *6* (1), 18867. https://doi.org/10.1038/srep18867.
(13) Bouit, P.-A.; Kamada, K.; Feneyrou, P.; Berginc, G.; Toupet, L.; Maury, O.; Andraud, C. Two-Photon Absorption-Related Properties of Functionalized BODIPY Dyes in the Infrared Range up to Telecommunication Wavelengths. *Adv. Mater.* **2009**, *21* (10–11), 1151–1154. https://doi.org/10.1002/adma.200801778.
(14) Sheng, W.; Zheng, Y.-Q.; Wu, Q.; Wu, Y.; Yu, C.; Jiao, L.; Hao, E.; Wang, J.-Y.; Pei, J. Synthesis, Properties, and Semiconducting Characteristics of BF $_2$ Complexes of β,β-Bisphenanthrene-Fused Azadipyrromethenes. *Org. Lett.* **2017**, *19* (11), 2893–2896. https://doi.org/10.1021/acs.orglett.7b01133.
(15) Sheng, W.; Cui, J.; Ruan, Z.; Yan, L.; Wu, Q.; Yu, C.; Wei, Y.; Hao, E.; Jiao, L. [*A*]-Phenanthrene-Fused BF $_2$ Azadipyrromethene (AzaBODIPY) Dyes as Bright Near-Infrared Fluorophores. *J. Org. Chem.* **2017**, *82* (19), 10341–10349. https://doi.org/10.1021/acs.joc.7b01803.
(16) Sheng, W.; Wu, Y.; Yu, C.; Bobadova-Parvanova, P.; Hao, E.; Jiao, L. Synthesis, Crystal Structure, and the Deep Near-Infrared Absorption/Emission of Bright AzaBODIPY-Based Organic Fluorophores. *Org. Lett.* **2018**, *20* (9), 2620–2623. https://doi.org/10.1021/acs.orglett.8b00820.
(17) Zheng, W.; Wang, B.-B.; Li, C.-H.; Zhang, J.-X.; Wan, C.-Z.; Huang, J.-H.; Liu, J.; Shen, Z.; You, X.-Z. Asymmetric Donor-π-Acceptor-Type Benzo-Fused Aza-BODIPYs: Facile Synthesis and Colorimetric Properties. *Angew. Chem. Int. Ed.* **2015**, *54* (31), 9070–9074. https://doi.org/10.1002/anie.201501984.
(18) Zhao, W.; Carreira, E. M. Conformationally Restricted Aza-BODIPY: Highly Fluorescent, Stable Near-Infrared Absorbing Dyes. *Chem. - Eur. J.* **2006**, *12* (27), 7254–7263. https://doi.org/10.1002/chem.200600527.
(19) David, S.; Chang, H.; Lopes, C.; Brännlund, C.; Le Guennic, B.; Berginc, G.; Van Stryland, E.; Bondar, M. V.; Hagan, D.; Jacquemin, D.; Andraud, C.; Maury, O. Benzothiadiazole-Substituted Aza-BODIPY Dyes: Two-Photon Absorption Enhancement for Improved Optical Limiting Performances in the Short-Wave IR Range. *Chem. – Eur. J.* **2021**, *27* (10), 3517–3525. https://doi.org/10.1002/chem.202004899.
(20) Berhe, S. A.; Rodriguez, M. T.; Park, E.; Nesterov, V. N.; Pan, H.; Youngblood, W. J. Optoelectronic Tuning of Organoborylazadipyrromethenes via Effective Electronegativity at the Metalloid Center. *Inorg. Chem.* **2014**, *53* (5), 2346–2348. https://doi.org/10.1021/ic402596u.
(21) Palma, A.; Tasior, M.; Frimannsson, D. O.; Vu, T. T.; Méallet-Renault, R.; O'Shea, D. F. New On-Bead Near-Infrared Fluorophores and Fluorescent Sensor Constructs. *Org. Lett.* **2009**, *11* (16), 3638–3641. https://doi.org/10.1021/ol901413u.
(22) Privat, M.; Bellaye, P.-S.; Lescure, R.; Massot, A.; Baffroy, O.; Moreau, M.; Racoeur, C.; Marcion, G.; Denat, F.; Bettaieb, A.; Collin, B.; Bodio, E.; Paul, C.; Goze, C. Development of an Easily Bioconjugatable Water-Soluble Single-Photon Emission-Computed Tomography/Optical Imaging Bimodal Imaging Probe Based on the Aza-BODIPY Fluorophore. *J. Med. Chem.* **2021**, *64* (15), 11063–11073. https://doi.org/10.1021/acs.jmedchem.1c00450.
(23) Florès, O.; Pliquett, J.; Abad Galan, L.; Lescure, R.; Denat, F.; Maury, O.; Pallier, A.; Bellaye, P.-S.; Collin, B.; Même, S.; Bonnet, C. S.; Bodio, E.; Goze, C. Aza-BODIPY Platform: Toward an Efficient Water-Soluble Bimodal Imaging Probe for MRI and Near-Infrared Fluorescence. *Inorg. Chem.* **2020**, *59* (2), 1306–1314. https://doi.org/10.1021/acs.inorgchem.9b03017.

(24) Kalot, G.; Godard, A.; Busser, B.; Pliquett, J.; Broekgaarden, M.; Motto-Ros, V.; Wegner, K. D.; Resch-Genger, U.; Köster, U.; Denat, F.; Coll, J.-L.; Bodio, E.; Goze, C.; Sancey, L. Aza-BODIPY: A New Vector for Enhanced Theranostic Boron Neutron Capture Therapy Applications. *Cells* **2020**, *9* (9), 1953. https://doi.org/10.3390/cells9091953.
(25) Lescure, R.; Privat, M.; Pliquett, J.; Massot, A.; Baffroy, O.; Busser, B.; Bellaye, P.-S.; Collin, B.; Denat, F.; Bettaïeb, A.; Sancey, L.; Paul, C.; Goze, C.; Bodio, E. Near-Infrared Emitting Fluorescent Homobimetallic Gold(I) Complexes Displaying Promising in Vitro and in Vivo Therapeutic Properties. *Eur. J. Med. Chem.* **2021**, *220*, 113483. https://doi.org/10.1016/j.ejmech.2021.113483.
(26) Lei, B.; Pan, H.; Zhang, Y.; Ren, X.-K.; Chen, Z. An Amphiphilic B,O-Chelated Aza-BODIPY Dye: Synthesis, PH-Sensitivity, and Aggregation Behaviour in a H_2O/DMSO Mixed Solvent. *Org. Biomol. Chem.* **2021**, *19* (27), 6108–6114. https://doi.org/10.1039/D1OB00746G.
(27) Jimenez, J. C.; Zhou, Z.; Rheingold, A. L.; Parker, S. M.; Sauvé, G. Tuning the Properties of Azadipyrromethene-Based Near-Infrared Dyes Using Intramolecular BO Chelation and Peripheral Substitutions. *Inorg. Chem.* **2021**, *60* (17), 13320–13331. https://doi.org/10.1021/acs.inorgchem.1c01597.
(28) Le Guennic, B.; Maury, O.; Jacquemin, D. Aza-Boron-Dipyrromethene Dyes: TD-DFT Benchmarks, Spectral Analysis and Design of Original near-IR Structures. *Phys Chem Chem Phys* **2012**, *14* (1), 157–164. https://doi.org/10.1039/C1CP22396H.
(29) Chibani, S.; Le Guennic, B.; Charaf-Eddin, A.; Maury, O.; Andraud, C.; Jacquemin, D. On the Computation of Adiabatic Energies in Aza-Boron-Dipyrromethene Dyes. *J. Chem. Theory Comput.* **2012**, *8* (9), 3303–3313. https://doi.org/10.1021/ct300618j.
(30) Loudet, A.; Bandichhor, R.; Burgess, K.; Palma, A.; McDonnell, S. O.; Hall, M. J.; O'Shea, D. F. *B* , *O* -Chelated Azadipyrromethenes as Near-IR Probes. *Org. Lett.* **2008**, *10* (21), 4771–4774. https://doi.org/10.1021/ol8018506.
(31) Fernando, R.; Pejić, S.; Thomsen, A.; Wang, C.; Sauvé, G. Azadipyrromethene-Based near-IR Dyes with Styryl Substituents at the Pyrrolic Positions for Organic Photovoltaic Applications. *Dyes Pigments* **2019**, *168*, 257–263. https://doi.org/10.1016/j.dyepig.2019.04.067.
(32) Bessette, A.; Cibian, M.; Ferreira, J. G.; DiMarco, B. N.; Bélanger, F.; Désilets, D.; Meyer, G. J.; Hanan, G. S. Azadipyrromethene Cyclometalation in Neutral Ru^{II} Complexes: Photosensitizers with Extended near-Infrared Absorption for Solar Energy Conversion Applications. *Dalton Trans.* **2016**, *45* (26), 10563–10576. https://doi.org/10.1039/C6DT00961A.
(33) Senevirathna, W.; Liao, J.; Mao, Z.; Gu, J.; Porter, M.; Wang, C.; Fernando, R.; Sauvé, G. Synthesis, Characterization and Photovoltaic Properties of Azadipyrromethene-Based Acceptors: Effect of Pyrrolic Substituents. *J. Mater. Chem. A* **2015**, *3* (8), 4203–4214. https://doi.org/10.1039/C4TA05765A.
(34) Senevirathna, W.; Sauvé, G. Introducing 3D Conjugated Acceptors with Intense Red Absorption: Homoleptic Metal(Ii) Complexes of Di(Phenylacetylene) Azadipyrromethene. *J. Mater. Chem. C* **2013**, *1* (40), 6684. https://doi.org/10.1039/c3tc31377h.
(35) Deligonul, N.; Gray, T. G. Azadipyrromethene Complexes of d^8 Metal Centers: Rhodium(I), Iridium(I), Palladium(II), and Platinum(II). *Inorg. Chem.* **2013**, *52* (22), 13048–13057. https://doi.org/10.1021/ic4017239.
(36) Teets, T. S.; Partyka, D. V.; Updegraff, J. B.; Gray, T. G. Homoleptic, Four-Coordinate Azadipyrromethene Complexes of d^{10} Zinc and Mercury. *Inorg. Chem.* **2008**, *47* (7), 2338–2346. https://doi.org/10.1021/ic701190g.
(37) Teets, T. S.; Partyka, D. V.; Esswein, A. J.; Updegraff, J. B.; Zeller, M.; Hunter, A. D.; Gray, T. G. Luminescent, Three-Coordinate Azadipyrromethene Complexes of d^{10} Copper, Silver, and Gold. *Inorg. Chem.* **2007**, *46* (16), 6218–6220. https://doi.org/10.1021/ic700776t.
(38) Thoi, V. S.; Stork, J. R.; Magde, D.; Cohen, S. M. Luminescent Dipyrrinato Complexes of Trivalent Group 13 Metal Ions. *Inorg. Chem.* **2006**, *45* (26), 10688–10697. https://doi.org/10.1021/ic061581h.

(39) Ikeda, C.; Ueda, S.; Nabeshima, T. Aluminium Complexes of N2O2-Type Dipyrrins: The First Hetero-Multinuclear Complexes of Metallo-Dipyrrins with High Fluorescence Quantum Yields. *Chem. Commun.* **2009**, No. 18, 2544. https://doi.org/10.1039/b820141b.
(40) Sumiyoshi, A.; Chiba, Y.; Matsuoka, R.; Noda, T.; Nabeshima, T. Efficient Luminescent Properties and Cation Recognition Ability of Heavy Group 13 Element Complexes of N_2O_2- and N_2O_4-Type Dipyrrins. *Dalton Trans.* **2019**, *48* (35), 13169–13175. https://doi.org/10.1039/C9DT02403D.
(41) Hansch, Corwin.; Leo, A.; Taft, R. W. A Survey of Hammett Substituent Constants and Resonance and Field Parameters. *Chem. Rev.* **1991**, *91* (2), 165–195. https://doi.org/10.1021/cr00002a004.
(42) Gorman, A.; Killoran, J.; O'Shea, C.; Kenna, T.; Gallagher, W. M.; O'Shea, D. F. In Vitro Demonstration of the Heavy-Atom Effect for Photodynamic Therapy. *J. Am. Chem. Soc.* **2004**, *126* (34), 10619–10631. https://doi.org/10.1021/ja047649e.
(43) Rurack, K.; Spieles, M. Fluorescence Quantum Yields of a Series of Red and Near-Infrared Dyes Emitting at 600−1000 Nm. *Anal. Chem.* **2011**, *83* (4), 1232–1242. https://doi.org/10.1021/ac101329h.
(44) Tyburski, R.; Liu, T.; Glover, S. D.; Hammarström, L. Proton-Coupled Electron Transfer Guidelines, Fair and Square. *J. Am. Chem. Soc.* **2021**, *143* (2), 560–576. https://doi.org/10.1021/jacs.0c09106.
(45) Fulmer, G. R.; Miller, A. J. M.; Sherden, N. H.; Gottlieb, H. E.; Nudelman, A.; Stoltz, B. M.; Bercaw, J. E.; Goldberg, K. I. NMR Chemical Shifts of Trace Impurities: Common Laboratory Solvents, Organics, and Gases in Deuterated Solvents Relevant to the Organometallic Chemist. *Organometallics* **2010**, *29* (9), 2176–2179. https://doi.org/10.1021/om100106e.
(46) Frisch, M. J.; Trucks, G. W.; Schlegel, H. B.; Scuseria, G. E.; Robb, M. A.; Cheeseman, J. R.; Scalmani, G.; Barone, V.; Petersson, G. A.; Nakatsuji, H.; Li, X.; Caricato, M.; Marenich, A. V.; Bloino, J.; Janesko, B. G.; Gomperts, R.; Mennucci, B.; Hratchian, H. P.; Ortiz, J. V.; Izmaylov, A. F.; Sonnenberg, J. L.; Williams; Ding, F.; Lipparini, F.; Egidi, F.; Goings, J.; Peng, B.; Petrone, A.; Henderson, T.; Ranasinghe, D.; Zakrzewski, V. G.; Gao, J.; Rega, N.; Zheng, G.; Liang, W.; Hada, M.; Ehara, M.; Toyota, K.; Fukuda, R.; Hasegawa, J.; Ishida, M.; Nakajima, T.; Honda, Y.; Kitao, O.; Nakai, H.; Vreven, T.; Throssell, K.; Montgomery Jr., J. A.; Peralta, J. E.; Ogliaro, F.; Bearpark, M. J.; Heyd, J. J.; Brothers, E. N.; Kudin, K. N.; Staroverov, V. N.; Keith, T. A.; Kobayashi, R.; Normand, J.; Raghavachari, K.; Rendell, A. P.; Burant, J. C.; Iyengar, S. S.; Tomasi, J.; Cossi, M.; Millam, J. M.; Klene, M.; Adamo, C.; Cammi, R.; Ochterski, J. W.; Martin, R. L.; Morokuma, K.; Farkas, O.; Foresman, J. B.; Fox, D. J. Gaussian 16 Rev. A.03, 2016.
(47) Adamo, C.; Barone, V. Toward Reliable Density Functional Methods without Adjustable Parameters: The PBE0 Model. *J. Chem. Phys.* **1999**, *110* (13), 6158–6170. https://doi.org/10.1063/1.478522.
(48) Scalmani, G.; Frisch, M. J. Continuous Surface Charge Polarizable Continuum Models of Solvation. I. General Formalism. *J. Chem. Phys.* **2010**, *132* (11), 114110. https://doi.org/10.1063/1.3359469.
(49) Sukumaran, S.; Chee, C.; Viswanathan, G.; Buckle, M.; Othman, R.; Abd. Rahman, N.; Chung, L. Synthesis, Biological Evaluation and Molecular Modelling of 2'-Hydroxychalcones as Acetylcholinesterase Inhibitors. *Molecules* **2016**, *21* (7), 955. https://doi.org/10.3390/molecules21070955.
(50) Loudet, A.; Bandichhor, R.; Burgess, K.; Palma, A.; McDonnell, S. O.; Hall, M. J.; O'Shea, D. F. *B*,*O*-Chelated Azadipyrromethenes as Near-IR Probes. *Org. Lett.* **2008**, *10* (21), 4771–4774. https://doi.org/10.1021/ol8018506.